

1 **Drivers of Future Extratropical Sea Surface**
2 **Temperature Variability Changes in the North Pacific**

3 **Jacob L. Gunnarson¹, Malte F. Stuecker^{1,2}, Sen Zhao³**

4 ¹Department of Oceanography, University of Hawai'i at Mānoa, Honolulu, HI, USA

5 ²International Pacific Research Center, University of Hawai'i at Mānoa, Honolulu, HI, USA

6 ³Department of Atmospheric Sciences, University of Hawai'i at Mānoa, Honolulu, HI, USA

7 **Key Points:**

- 8 • We propose a method to diagnose the drivers of projected future changes to ex-
9 tratropical sea surface temperature variance
- 10 • These sea surface temperature variance changes are spatially heterogeneous in the
11 Community Earth System Model version 2 large ensemble
- 12 • Changes in the North Pacific are largely driven by El Niño teleconnection shifts,
13 augmented by ocean memory and stochastic forcing changes

Corresponding author: Jacob L. Gunnarson, jlgunnar@hawaii.edu

Abstract

Under anthropogenic warming, future changes to climate variability beyond specific modes such as the El Niño-Southern Oscillation (ENSO) have not been well-characterized. In the Community Earth System Model version 2 Large Ensemble (CESM2-LE) climate model, the future change to sea surface temperature (SST) variability is spatially heterogeneous. We examined these projected changes (between 1960-2000 and 2060-2100) in the North Pacific using a local linear stochastic-deterministic model, which allowed us to quantify the effect of changes to three drivers on SST variability: ocean “memory” (the SST damping timescale), ENSO teleconnections, and stochastic noise forcing. The ocean memory declines in most areas, but lengthens in the central North Pacific. This change is primarily due to changes in air-sea feedbacks and ocean damping, with the shallowing mixed layer depth playing a secondary role. An eastward shift of the ENSO teleconnection pattern is primarily responsible for the pattern of SST variance change.

Plain Language Summary

In this study we investigated the physical reasons why fluctuations of sea surface temperatures – i.e., variations from the seasonal cycle – change as the world warms. These changes are important because extreme fluctuations above the normal state, so-called marine heat waves, can have severe ecological and economic impacts. Combining a conceptual model with a state-of-the-art climate model, we examined the reasons why sea surface temperature variability in the North Pacific is projected to change heterogeneously: some areas experience higher variability in the future, some less. Three different processes are important: ocean memory (i.e., how long temperature anomalies persist), the remote influence of El Niño, and the random weather variations in the atmosphere. While changes in all three processes affect future sea surface temperature variability changes, geographical shifts in how El Niño affects the upper ocean’s temperature are the most important.

1 Introduction

Anthropogenic emissions of greenhouse gasses are causing profound changes to the Earth’s climate. Changes to the climate mean state have been studied for over half a century (e.g., Manabe and Wetherald (1967)) and are often used to set targets for reducing greenhouse gas emissions. In contrast, changes to climate variability—characterized

44 statistically by variance and occurrence of extreme events and of importance for regional
45 adaptation strategies—under future warming scenarios are less well understood.

46 There is a substantial body of literature characterizing future changes to specific
47 modes of climate variability such as the El Niño-Southern Oscillation (ENSO) (Cai et
48 al., 2020; Cai et al., 2018; Geng et al., 2022; Maher et al., 2023; Timmermann et al., 1999;
49 Wengel et al., 2021; Ying et al., 2022) and the Madden-Julian Oscillation (Bui & Mal-
50 oney, 2018, 2020; Jenney et al., 2021; Rushley et al., 2019). However the broader study
51 of climate variability changes is an emerging field with many outstanding questions (Rodgers
52 et al., 2021; Stouffer & Wetherald, 2007; van der Wiel & Bintanja, 2021).

53 The recent advent of large ensemble climate model simulations offers an opportu-
54 nity to robustly quantify future variance and extreme event changes (Deser et al., 2020;
55 Li et al., 2021; Maher et al., 2019; Rodgers et al., 2021). Conducting a large number of
56 simulations with the same climate model with identical external forcing but perturbed
57 initial conditions allows for a clear identification of the forced signal as it changes over
58 time, leaving only model and scenario uncertainty (Hawkins & Sutton, 2009).

59 In this study, we examined the projected change to sea surface temperature (SST)
60 variability in the North Pacific and its physical drivers using the Community Earth Sys-
61 tem Model version 2 Large Ensemble (CESM2-LE), which consists of 100 ensemble mem-
62 ber simulations (Rodgers et al., 2021). Changes to SST variability are of key importance
63 to both physical and biological components of the climate system: SSTs couple the ocean
64 and atmosphere via radiative and turbulent heat fluxes (Deser et al., 2010) and control
65 many physiological processes of marine organisms (Smith et al., 2023). The occurrence
66 of marine heatwaves, prolonged periods of anomalously high SST that result in severe
67 ecological and socioeconomic impacts (Smith et al., 2021), is directly related to SST vari-
68 ability from a moving baseline perspective (Amaya et al., 2023; Oliver et al., 2021).

69 Strikingly, the projected change in SST variance in CESM2-LE between 1960-2000
70 and 2060-2100 is not spatially uniform (Figure 1c), and the aim of this study was to iden-
71 tify the drivers responsible for this pattern of variability change. Note that these pro-
72 jected changes in variance will directly translate (if the other statistical moments remain
73 constant) to changes of threshold exceedances of upper percentiles (e.g., the 90th per-
74 centile) that are often used to define marine heatwaves (e.g., Jacox et al. (2020)). Thus
75 our results have direct applicability to the study of future marine heat wave changes. We

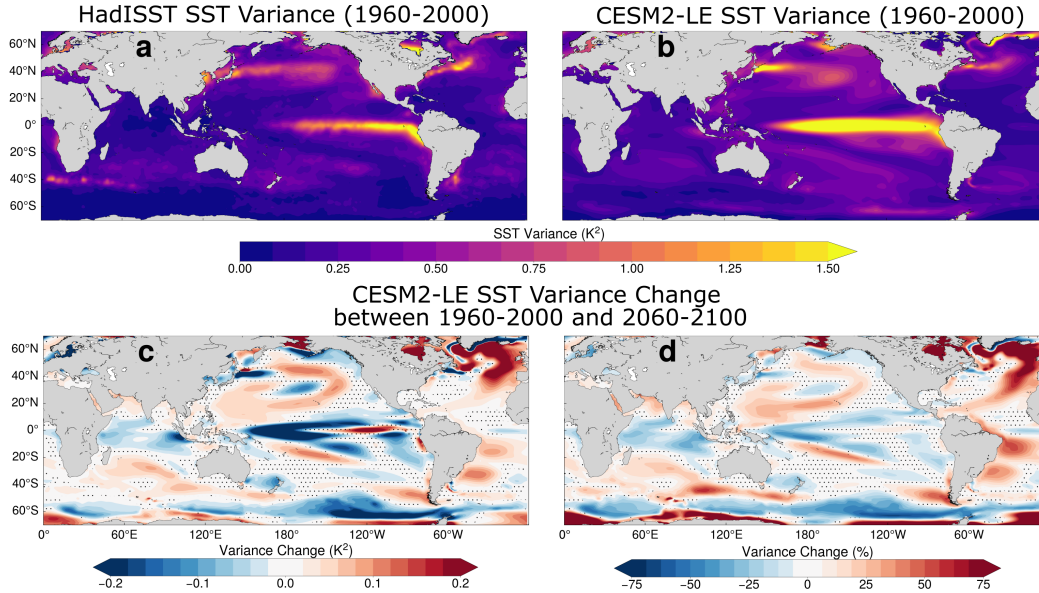


Figure 1. (a) SST variance during 1960-2000 from HadISST and (b) from CESM2-LE. (c) SST variance change in CESM2-LE between 1960-2000 and 2060-2100. (d) Relative SST variance change between those time periods. Stippled areas in (c) and (d) show where the change in variance is not significant at the 5% level.

76 used a local linear stochastic SST model to quantify the relative effect of changes to three
 77 drivers on the overall change in SST variance: ocean memory, ENSO teleconnections,
 78 and stochastic noise forcing.

79 2 Methods

80 2.1 Data

81 We used the Community Earth System Model version 2 Large Ensemble in this study.
 82 CESM2 is a coupled Earth system model with active ocean biogeochemistry (Danaba-
 83 soglu et al., 2020). The model incorporates the CAM6 atmosphere model and POP2 ocean
 84 model, both on $\sim 1^\circ$ horizontal grids, as well as coupled land, sea ice, wave, marine bio-
 85 geochemical, and river runoff models. The large ensemble consists of 100 ensemble mem-
 86 bers run from 1850 to 2100 and forced by CMIP6 historical (1850-2014) and SSP3-7.0
 87 protocols (2015-2100) (Rodgers et al., 2021). The SSP3-7.0 scenario, which has a high
 88 rate of emissions, was selected to investigate climate variability and its projected future
 89 changes. Anomalies were calculated by subtracting the ensemble mean from each ensem-

90 ble member. We excluded SST data from our analysis at grid points where the ensemble-
91 mean sea ice fraction exceeded 15% for any month during the time period considered.

92 Additionally we used several observational and reanalysis products to compare the
93 CESM2-LE results in the historical period (1960-2000 unless otherwise noted). We used
94 SSTs from the Hadley Centre Global Sea Ice and Sea Surface Temperature v1.1 dataset
95 (HadISST; Rayner (2003)); sea level pressure and 850-hPa winds from the ECMWF Re-
96 analysis v5 (ERA5; Hersbach et al. (2020)); mixed layer depth from the Ocean Reanal-
97 ysis System 5 (ORAS5; Zuo et al. (2019)), which is defined as the depth where the den-
98 sity exceeds the near surface density by 0.01 kg m^{-3} ; turbulent surface heat fluxes from
99 the 1° Objectively Analyzed air-sea Fluxes (OAFLUX; Yu and Weller (2007)); and ra-
100 diative surface heat fluxes from OAFLUX (derived from the ISCCP-D product; Rossow
101 and Schiffer (1999)) and Clouds and Earth's Radiant Energy Systems Energy Balanced
102 and Filled Ed4.2 product (CERES EBAF; Kato et al. (2018)). Anomalies were calcu-
103 lated by subtracting the climatology for the entire time period used and then detrend-
104 ing with a linear fit. We excluded HadISST data from our analysis at grid points with
105 sea ice cover (i.e., NaN values in the data) during any month from January 1960 to Jan-
106 uary 2000.

107 For the radiative heat fluxes, we calculated anomalies separately for OAFLUX (Jan-
108 uary 1985 to February 2000) and CERES EBAF (March 2000 to December 2022), and
109 then combined the two sets of anomalies. We spatially smoothed this heat flux data us-
110 ing a moving average filter with 3-by-3-grid-cell window size. For computations requir-
111 ing both heat flux and SST data, we also spatially smoothed the HadISST data in the
112 same manner. Note that the CESM2-LE data was not smoothed.

113 **2.2 Linear Stochastic-Deterministic Model**

114 To quantify the effect of different drivers on SST variance, we used an extension
115 of the original local linear stochastic climate model (Frankignoul & Hasselmann, 1977;
116 Hasselmann, 1976) with seasonally modulated feedback and noise forcing (De Elvira &
117 Lemke, 1982; Nicholls, 1984) and an ENSO teleconnection term (Newman et al., 2016;
118 Newman et al., 2003; Schneider & Cornuelle, 2005). We use the formulation developed
119 by Stuecker (2023), Stuecker et al. (2017), and Zhao et al. (2019) that includes seasonal

120 modulations in the feedback, noise forcing, and the ENSO teleconnection term:

$$121 \quad \frac{\partial T'(t)}{\partial t} = \tilde{\lambda}T'(t) + \tilde{\beta}N(t) + \xi(t), \quad (1)$$

122 where T' is the SST anomaly at a given location, $\tilde{\lambda}$ is a seasonally modulated feedback
 123 coefficient, $\tilde{\beta}$ is a seasonally modulated ENSO teleconnection coefficient, N is the Niño3.4
 124 index (the SST anomaly averaged over 5°N-5°S, 170°W-120°W), and ξ is stochastic forc-
 125 ing (i.e., “weather noise”). Averaged over the annual cycle, $\tilde{\lambda}$ must be negative so that
 126 SST anomalies are damped and do not grow without bound. $\tilde{\lambda}^{-1}$ has units of time and
 127 represents the decay timescale of SST anomalies, thus we refer to it hereafter to as the
 128 “ocean memory” (Shi et al., 2022).

129 The parameters $\tilde{\lambda}$ and $\tilde{\beta}$ are defined as

$$130 \quad \tilde{\lambda} = \lambda_0 + \lambda_1 \sin(\omega_a t) + \lambda_2 \cos(\omega_a t), \quad (2)$$

$$131 \quad \tilde{\beta} = \beta_0 + \beta_1 \sin(\omega_a t) + \beta_2 \cos(\omega_a t), \quad (3)$$

132 where ω_a is the angular frequency of the annual cycle ($2\pi/12$ months⁻¹) and λ_1 , λ_2 , β_1 ,
 133 and β_2 determine the amplitude and phase of the seasonal modulation. Physically, the
 134 seasonal modulation of these coefficients reflects seasonal changes of air-sea heat fluxes
 135 and the mixed layer heat capacity, the latter which is proportional to the mixed layer
 136 depth (Frankignoul et al., 2002; Stuecker et al., 2017). For ease of display we present these
 137 coefficients as annual averages in this report (the amplitude and phase of $\tilde{\lambda}$ and $\tilde{\beta}$ are
 138 shown in Figure S1 in the Supporting Information).

139 The noise term ξ represents stochastic forcing from the atmosphere. It includes all
 140 processes that are uncorrelated with local SST anomalies and remote ENSO forcing, pri-
 141 marily anomalous air-sea heat fluxes and anomalous Ekman advection of the SST gra-
 142 dient due to weather variability (Larson et al., 2018). ξ should be nearly white given the
 143 fast decorrelation timescale of the atmosphere (Hasselmann, 1976; Lorenz, 1963).

144 At each grid point for each ensemble member, equation 1 was fitted to the SST anomaly
 145 data using multiple linear regression (see Zhao et al., 2019). $\partial T'/\partial t$ was computed us-
 146 ing the forward finite difference method. The noise forcing ξ was taken to be the resid-
 147 ual from the fit. This residual is well-described by white noise (see Figure S2 in the Sup-
 148 porting Information), supporting the suitability of our choice of theoretical SST model.

149

2.3 SST Feedback Decomposition

150

151

The SST feedback coefficient $\tilde{\lambda}$ is the sum of several different atmospheric and oceanic feedbacks (Frankignoul, 1985; Haney, 1971; Patrizio & Thompson, 2021, 2022):

152

$$\tilde{\lambda} = \tilde{\lambda}_{\text{SH}} + \tilde{\lambda}_{\text{LH}} + \tilde{\lambda}_{\text{SW}} + \tilde{\lambda}_{\text{LW}} + \tilde{\lambda}_{\text{ent}} + \tilde{\lambda}_{\text{diff}} + \tilde{\lambda}_{\text{other}} \quad (4)$$

153

154

155

156

157

where $\tilde{\lambda}_{\text{SH}}$, $\tilde{\lambda}_{\text{LH}}$, $\tilde{\lambda}_{\text{SW}}$, $\tilde{\lambda}_{\text{LW}}$ are the feedbacks associated with the sensible, latent, short-wave, and longwave components of the air-sea heat flux, respectively; $\tilde{\lambda}_{\text{ent}}$ is the feedback due to entrainment as the mixed layer deepens in fall and winter; $\tilde{\lambda}_{\text{diff}}$ is the feedback due to horizontal eddy diffusion, and $\tilde{\lambda}_{\text{other}}$ is the feedback due to non-local and other processes not considered here.

158

159

We calculate the air-sea heat flux feedbacks given heat flux component x by fitting the following equation using multiple linear regression:

160

$$Q'_x(t) = \tilde{\lambda}_x^* T'(t) + \tilde{\beta}_x^* N(t) + \xi_x^*(t), \quad (5)$$

161

162

163

where $Q'_x(t)$ is the heat flux anomaly (defined as positive downward), $\tilde{\lambda}_x^*$ is the feedback for that heat flux component (with units $\text{Wm}^{-2}\text{K}^{-1}$), and $\xi_x^*(t)$ is the noise forcing. $\tilde{\lambda}_x^*$ is related to the feedbacks $\tilde{\lambda}_x$ in equation 4 by the following:

164

$$\tilde{\lambda}_x = \frac{\tilde{\lambda}_x^*}{\rho c_p \tilde{H}} \quad (6)$$

165

166

167

168

169

where ρ is the density of seawater (1024 kg m^{-3}), c_p is the heat capacity of seawater ($4001 \text{ J kg}^{-1} \text{ K}^{-1}$), and \tilde{H} is the monthly mixed layer depth climatology. To fit this equation to observations, we used the whole time period available for the heat flux data to minimize the error: January 1985 to December 2022 instead of the 1960-2000 period for fitting equation 1.

170

The feedback due to entrainment is

171

$$\tilde{\lambda}_{\text{ent}} = -\frac{\tilde{w}_{\text{ent}}}{\tilde{H}} \left(1 - \left\langle \frac{\partial T'_b}{\partial T'} \right\rangle \right), \quad (7)$$

172

173

174

175

176

177

where \tilde{w}_{ent} is the entrainment velocity climatology, the time derivative of the mixed layer depth climatology \tilde{H} , and T'_b is the temperature below the mixed layer, with angled brackets denoting the ensemble/time mean (see Frankignoul (1985)). If T'_b is uncorrelated with T' , and assuming a mixed layer of average depth 75 meters with an annual cycle amplitude of 100 meters, $\tilde{\lambda}_{\text{ent}} \approx -0.1 \text{ months}^{-1}$ when averaged over the annual cycle. Entrainment also leads to the phenomenon of “reemergence”: often the SST anomaly from

178 the previous winter persists under the mixed layer during summer and in fall is re-entrained
 179 into the mixed layer, leading to the reemergence of SST anomalies (Alexander & Deser,
 180 1995; Deser et al., 2003). Reemergence is not modeled in this work.

181 The feedback due to horizontal eddy diffusion is

$$182 \quad \tilde{\lambda}_{\text{diff}} = \frac{\partial}{\partial T'} \left(\kappa \nabla^2 T' \right), \quad (8)$$

183 where κ is the horizontal eddy diffusivity. Assuming SST anomalies with a sinusoidal
 184 spatial structure of wavelength L , the feedback can be estimated via scaling analysis as

$$185 \quad \tilde{\lambda}_{\text{diff}} \approx -\kappa \frac{4\pi^2}{L^2}. \quad (9)$$

186 For $L \approx 1000$ km (i.e., a length scale of ~ 160 km) and $\kappa \approx 500 \text{ m}^2\text{s}^{-1}$ (note that κ is
 187 a function of length scale and geographic location; see Nummelin et al. (2021)), $\lambda_{\text{diff}} \approx$
 188 $-0.05 \text{ months}^{-1}$.

189 Equation 4 can be rewritten as

$$190 \quad \tilde{\lambda} = \frac{\tilde{\lambda}_{\text{turb}}^*}{\rho c_p \tilde{H}} + \frac{\tilde{\lambda}_{\text{rad}}^*}{\rho c_p \tilde{H}} + \tilde{\lambda}_{\text{res}}, \quad (10)$$

191 where $\tilde{\lambda}_{\text{turb}}^*$ is the turbulent ($\tilde{\lambda}_{\text{SH}}^* + \tilde{\lambda}_{\text{LH}}^*$) heat flux feedback, $\tilde{\lambda}_{\text{rad}}^*$ is the radiative ($\tilde{\lambda}_{\text{SW}}^* + \tilde{\lambda}_{\text{LW}}^*$)
 192 heat flux feedback, and $\tilde{\lambda}_{\text{res}}$ is the residual feedback. $\tilde{\lambda}_{\text{res}}$ includes $\tilde{\lambda}_{\text{ent}}$, $\tilde{\lambda}_{\text{diff}}$, $\tilde{\lambda}_{\text{other}}$, and
 193 errors in estimating the air-sea feedbacks. From the estimations above, $\tilde{\lambda}_{\text{ent}} + \tilde{\lambda}_{\text{diff}} \approx -0.15$
 194 months^{-1} , thus we expect $\tilde{\lambda}_{\text{res}}$ to have a similar value if there are not substantial errors
 195 in the calculation of the feedbacks and contributions from other unmodeled feedbacks.
 196 Because the large number of degrees of freedom in CESM2-LE (100 members) allows for
 197 robust statistical estimates of the atmospheric feedbacks, we expect $\tilde{\lambda}_{\text{res}}$ to primarily re-
 198 flect damping by entrainment and diffusion. However, for observations/reanalysis, un-
 199 certainties in the heat flux, SST, and mixed layer depth data may compound to produce
 200 substantial errors in the calculated feedbacks and thus $\tilde{\lambda}_{\text{res}}$ may primarily reflect these
 201 errors rather than just damping from oceanic processes.

202 The change in the feedback can be expanded from equation 10 as

$$203 \quad \Delta \tilde{\lambda} = \frac{\Delta \tilde{\lambda}_{\text{turb}}^*}{\rho c_p \tilde{H}_0} + \frac{\Delta \tilde{\lambda}_{\text{rad}}^*}{\rho c_p \tilde{H}_0} + \underbrace{\frac{-\tilde{\lambda}_{\text{turb},0}^* - \tilde{\lambda}_{\text{rad},0}^*}{\rho c_p \tilde{H}_0^2}}_{\Delta \tilde{\lambda}_H} \Delta \tilde{H} + \Delta \tilde{\lambda}_{\text{res}}, \quad (11)$$

204 where Δ indicates the change between the two time periods, a subscript 0 indicates that
 205 the value from the first time period is used and $\Delta \tilde{\lambda}_H$ is the change in the air-sea heat
 206 flux feedback due to the change in the mixed layer depth climatology.

2.4 Applicability of the Linear Stochastic-Deterministic Model

Equation 1 describes SSTs forced solely by the atmosphere: anomalous air-sea heat fluxes and anomalous Ekman advection of the mean SST gradient from stochastic weather processes and remote forcing from ENSO. Contributions to the variance from internal ocean dynamics (e.g., geostrophic advection, mixed layer depth variability, and entrainment) are neglected (Frankignoul & Reynolds, 1983). This simplification is inadequate to explain SST variance in the equatorial oceans, where coupled ocean-atmosphere dynamics in the Pacific give rise to ENSO; in western boundary currents, where ocean dynamics are important (Qiu, 2002; Reynolds, 1978; Schneider & Miller, 2001); and in the areas of the North Atlantic and Southern Ocean where the thermohaline circulation contributes to SST variability on long timescales (Delworth & Greatbatch, 2000; Zhang et al., 2019).

In previous studies, the applicability of a linear stochastic model to SST dynamics was tested by goodness of fit to a theoretical power spectrum (Frankignoul, 1985; Reynolds, 1978), by establishing a threshold of sea surface height variance over which oceanic processes were assumed to dominate (Hall & Manabe, 1997), or by comparing advection of SST anomalies with the estimated feedback term (Frankignoul et al., 2002).

We used an objective criterion based on the lagged covariance of SST anomalies T' and net surface heat flux anomalies Q' , R_{TQ} (see Frankignoul and Kestenare, 2002; Frankignoul, 1985; Frankignoul and Reynolds, 1983). If SST anomalies are both damped and forced by Q' , at negative lags (when the ocean leads), R_{TQ} should be negative, corresponding to damping of SST anomalies by Q' . At positive lags (when the atmosphere leads), R_{TQ} should be positive, corresponding to forcing of SST anomalies by Q' . Thus we considered that any grid point which had $R_{TQ} < 0$ at negative lags (averaged over lags -3 to -1 months and all ensemble members) and $R_{TQ} > 0$ at positive lags (averaged over lags 1 to 3 months and all ensemble members) to be well represented by a linear stochastic model forced by the atmosphere. The grid points that did not meet this criterion were excluded from our analysis and are shown as white hashed areas in the figures. As expected these grid points are in areas of high oceanic variability and strong air-sea coupling, such as the equatorial Pacific and Kuroshio-Oyashio Extension region. For observations, as with the calculation of the air-sea heat flux feedbacks, this criteria

238 was evaluated using data from January 1985 to December 2022. Figure S3 in the Sup-
 239 porting Information shows R_{TQ} at several representative locations.

240 2.5 Isolating SST Variance Contribution from Each Driver

241 Once $\tilde{\lambda}$, $\tilde{\beta}$, and ξ are determined, the SST variance due to changes in the correspond-
 242 ing drivers—the ocean memory, ENSO teleconnection, and noise forcing—can be isolated.
 243 We used two forward integrations, one isolating the SST anomalies forced only by the
 244 ENSO teleconnection T'_N and the other isolating SST anomalies forced only by noise T'_ξ :

$$245 T'_{N,k+1} = T'_{N,k} + (\tilde{\lambda}_k T'_{N,k} + \tilde{\beta}_k N_k) \Delta t, \quad (12)$$

$$246 T'_{\xi,k+1} = T'_{\xi,k} + (\tilde{\lambda}_k T'_{\xi,k} + \xi_k) \Delta t, \quad (13)$$

247 where k is the time index and Δt is the time step (one month). ξ_k was constructed us-
 248 ing a shuffled fit residual (for each ensemble member): for each calendar month, the year
 249 was randomly shuffled, producing noise forcing that is temporally uncorrelated (i.e., white)
 250 but retains spatial correlations and seasonal variance modulation present in the fit resid-
 251 ual. Our results differ little if the original fit residual (that contains both spatial corre-
 252 lations and a slight temporal autocorrelation) or a version in which the time dimension
 253 of the noise forcing is shuffled in a different random order at each grid point (and thus
 254 is white in both time and space; see Figure S4 in the Supporting Information).

255 We performed these integrations at each grid point and ensemble member for the
 256 following cases:

- 257 • $T'_{N,A}$ using $\tilde{\lambda}$, $\tilde{\beta}$, and $N(t)$ at their 1960-2000 values
- 258 • $T'_{\xi,A}$ using $\tilde{\lambda}$ and $\xi(t)$ at their 1960-2000 values
- 259 • $T'_{N,B}$ using $\tilde{\lambda}$, $\tilde{\beta}$, and $N(t)$ at their 2060-2100 values
- 260 • $T'_{\xi,B}$ using $\tilde{\lambda}$ and $\xi(t)$ at their 2060-2100 values
- 261 • $T'_{N,C}$ using $\tilde{\lambda}$ at its 1960-2000 values, and $\tilde{\beta}$ and $N(t)$ at their 2060-2100 values
- 262 • $T'_{\xi,C}$ using $\tilde{\lambda}$ at its 1960-2000 values and $\xi(t)$ at its 2060-2100 values

263 Each integration was initialized with the SST anomaly at the beginning of the specified
 264 time period (2060-2100 for case C). We calculated the change in variance due to the change

265 in each driver using the following expressions:

$$266 \quad \Delta^\lambda \sigma^2(T') = \left[\sigma^2(T'_{N,B}) + \sigma^2(T'_{\xi,B}) \right] - \left[\sigma^2(T'_{N,C}) + \sigma^2(T'_{\xi,C}) \right], \quad (14)$$

$$267 \quad \Delta^N \sigma^2(T') = \sigma^2(T'_{N,C}) - \sigma^2(T'_{N,A}), \quad (15)$$

$$268 \quad \Delta^\xi \sigma^2(T') = \sigma^2(T'_{\xi,C}) - \sigma^2(T'_{\xi,A}), \quad (16)$$

269 where $\Delta^x \sigma^2(T')$ is the change in SST variance due to changes to the driver x , $\sigma^2(T'_{x,n})$
 270 is the variance of the integrated SST time series corresponding to the case letter n (A,
 271 B, or C) above.

272 **2.6 Statistical Significance Testing**

273 All parameters shown in this report (e.g., $\sigma^2(T'_{x,n})$, $\tilde{\lambda}$, $\tilde{\beta}$) were calculated for each
 274 ensemble member, creating 100 independent samples. Welch's t -test was then used to
 275 assess the statistical significance of ensemble-mean changes of these parameters between
 276 1960-2000 and 2060-2100 (Welch, 1947). Except in areas with minimal changes, the null
 277 hypothesis of no change between the two time periods is rejected at the 5% level.

278 **3 Results & Discussion**

279 **3.1 Ocean Memory and Its Future Changes**

280 The ocean memory varies considerably across the North Pacific, both in observa-
 281 tions and CESM2. Over most of the North Pacific, the ocean memory diagnosed from
 282 the observations is between 2-6 months (Figure 2a). Equatorward of about 20°N, par-
 283 ticularly toward the eastern side the basin, the ocean memory is substantially longer,
 284 typically around 9 months. The magnitude of the ocean memory is largely consistent with
 285 previous estimations (e.g., Frankignoul and Reynolds (1983) and Schneider and Cornuelle
 286 (2005)) and the autocorrelation timescale of large-scale modes such as the the Pacific
 287 Decadal Oscillation (Newman et al., 2016).

288 In the observations, the contribution of the different heat fluxes to the total feed-
 289 back (Figure 3a-c) shows strong damping from turbulent heat fluxes (almost entirely the
 290 latent heat feedback) particularly in a band at 25°N in the western North Pacific. Over
 291 much of the North Pacific poleward of 20°N, the radiative heat flux feedback (almost
 292 entirely shortwave feedback) is positive, indicative of the low cloud-SST feedback, where
 293 negative SST anomalies are associated with increased atmospheric stability, leading to

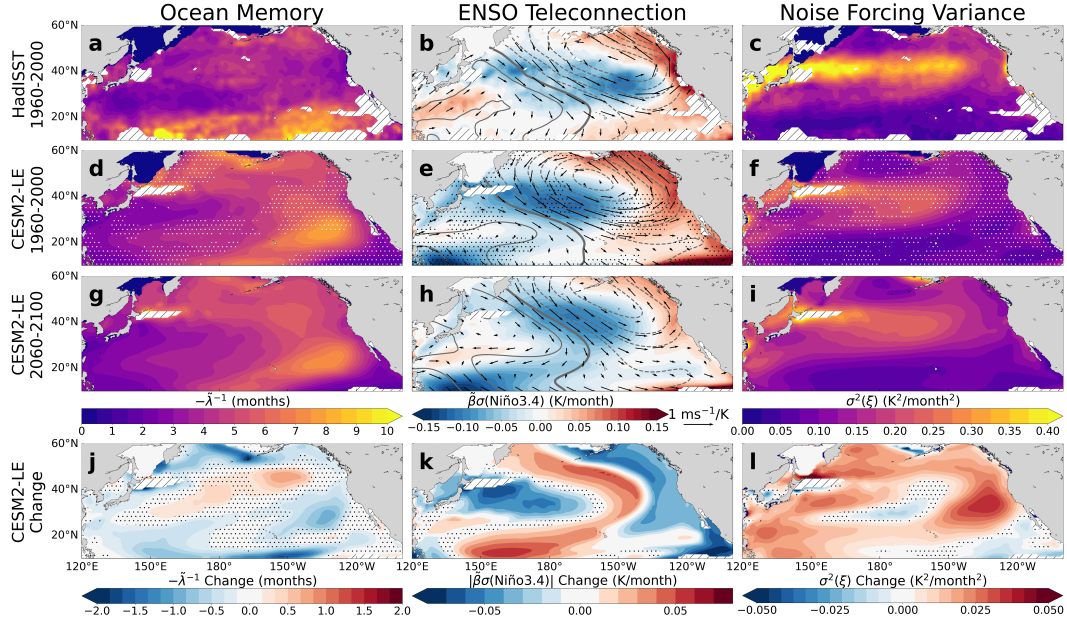


Figure 2. Equation 1 parameters fit to HadISST (a)-(c) and CESM2-LE (d)-(i) SST data in shaded contours, with CESM2-LE projected changes on the bottom row (j)-(l). (b), (e), (h) vectors and contours are the 850-hPa winds and sea level pressure regressed onto the Niño3.4 index, the latter with 0.25-hPa/K spacing (positive values are solid lines and negative lines are dashed, with a thicker line at the zero contour). Stippling in (d)-(f) indicates that the parameters derived from observations lie outside the 5th-95th percentile range of those derived from the CESM2-LE ensemble members. Stippling in (j)-(l) indicates where the changes are not significant at the 5% level. The ocean memory and ENSO teleconnection panels show the mean over the seasonal cycle, and all CESM2-LE panels are the ensemble mean. Locations where the SST data is not well-described by a local linear stochastic model are shown as white hatched areas (see Section 2.4).

294 the formation of low clouds which reduce surface shortwave radiation and further cool
 295 the ocean (Clement et al., 2009; Norris & Leovy, 1994; Xie, 2023).

296 The ocean memory in CESM2-LE is similar in magnitude to observations, rang-
 297 ing between about 2 and 9 months, but has a distinct spatial pattern (Figure 2d, g). The
 298 ocean memory is shorter in the western North Pacific than in the east, which can mostly
 299 be attributed to strong damping by turbulent heat fluxes (Figure 3d). As in the obser-
 300 vations, the turbulent and radiative feedbacks are dominated by the latent heat and short-
 301 wave feedbacks, respectively (see Figure S5 in the Supporting Information). A large area

302 of particularly long ocean memory is present between Hawai'i and North America, re-
 303 sulting from relatively weak turbulent heat flux damping and positive radiative feedback,
 304 likely from the low cloud-SST feedback.

305 Interestingly, the phases of $\tilde{\lambda}$ and \tilde{H} differ: $\tilde{\lambda}$ is most strongly negative between Au-
 306 gust and December (depending on location) whereas \tilde{H} is deepest between December
 307 and March (see Figure S1 in the Supporting Information). That implies that the sea-
 308 sonality of the air-sea heat flux feedbacks play a strong role in the seasonal modulation
 309 of $\tilde{\lambda}$ in addition to that of the mixed layer depth.

310 In observations, the residual feedback has considerable spatial structure (Figure
 311 3c), with areas of negative and strongly positive feedbacks. In CESM2-LE, the residual
 312 feedback is negative everywhere except for coastal areas off China and Mexico. As re-
 313 lated in Section 2.2, entrainment and horizontal eddy diffusion are expected to damp SST
 314 anomalies, with a combined feedback on the order of $-0.15 \text{ months}^{-1}$, which corresponds
 315 well with the results from CESM2-LE. However, the strong positive feedbacks in obser-
 316 vations could be the result of errors in the heat flux and mixed layer depth data. The
 317 magnitude of the feedbacks $\tilde{\lambda}_x^*$ for different heat flux components are similar between
 318 observations and CESM2-LE (see Figure S5 in the Supporting Information). However,
 319 the mixed layer depth is typically somewhat deeper in CESM2-LE than in the ORAS5
 320 reanalysis, which would lead to the $\tilde{\lambda}_{\text{rad}}$ and $\tilde{\lambda}_{\text{urb}}$ being greater in magnitude in obser-
 321 vations compared to CESM2-LE. Part of that discrepancy may be due to the different
 322 mixed layer definitions used: a density-based definition for ORAS5 (see Section 2.1) and
 323 a buoyancy-based definition for CESM2 (Large et al., 1997).

324 In the future climate in CESM2-LE, the ocean memory declines over most of the
 325 basin except for a zonally-elongated area in the central North Pacific where it increases
 326 (Figure 2j). The changes to the individual feedbacks are are spatially varied, but it ap-
 327 pears that the change in ocean memory is primarily driven by changes to the radiative
 328 and residual feedbacks, suggesting that changes in clouds and ocean dynamics are most
 329 important for the change in ocean memory. In common with other climate models (e.g.,
 330 Capotondi et al. (2012) and Shi et al. (2022)), the mixed layer depth in the North Pa-
 331 cific in CESM2-LE is shallower nearly everywhere in the future climate, leading to a re-
 332 duced heat capacity and correspondingly shorter ocean memory (Figure 3g). However,
 333 the magnitude of the feedback change due to the shallower mixed layer is relatively mi-

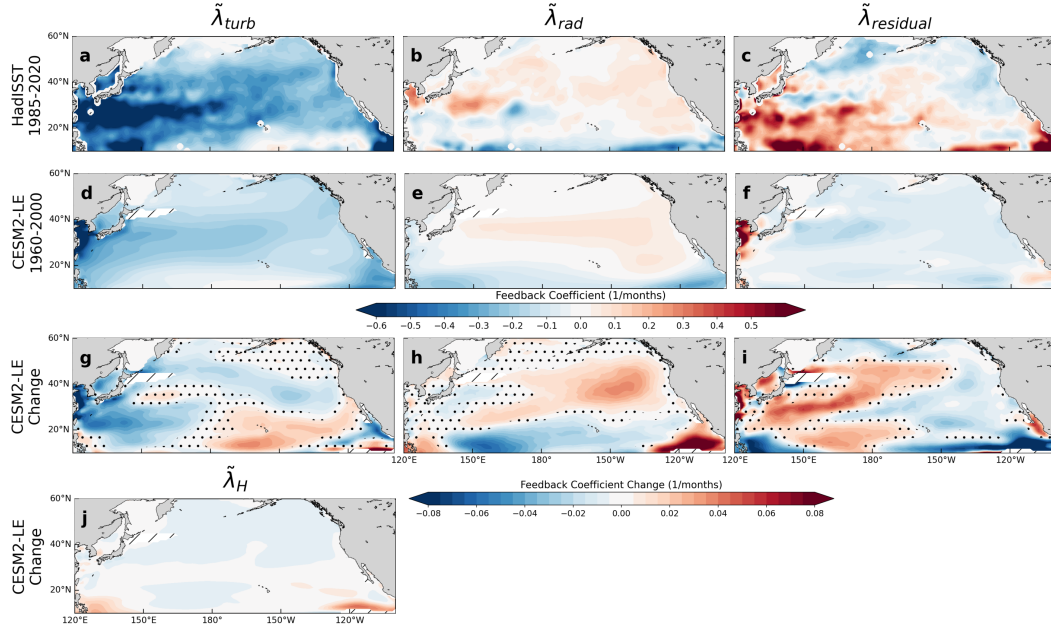


Figure 3. (a)-(f) Turbulent, radiative, and residual SST feedbacks in HadISST and CESM2-LE for 1960-2000. (g)-(i) Changes to those feedbacks in CESM2-LE between 1960-2000 and 2060-2100, with (j) showing the contribution of the mixed layer depth change. Stippling in (g)-(i) indicates where the changes are not significant at the 5% level. All panels show the feedbacks averaged over the seasonal cycle and the CESM2-LE panels showing the ensemble mean. Locations where the SST data does not meet the criterion described in Section 2.4 are shown as white hatched areas.

334 nor compared to the changes to the other feedbacks, in contrast with the findings of Shi
 335 et al. (2022), who attributed the projected decline in ocean memory in CMIP6 models
 336 primarily to mixed layer depth shallowing.

337 3.2 ENSO Teleconnection and Its Future Changes

338 The ENSO teleconnection, represented by $\tilde{\beta}$ multiplied by the standard deviation
 339 of Niño3.4, in both observations and CESM2-LE (Figure 2b, e, h) exhibits the well-known
 340 "atmospheric bridge" pattern: cooling (warming) of SSTs in the central North Pacific
 341 and warming (cooling) in the eastern North Pacific during El Niño (La Niña) (Alexan-
 342 der et al., 2002; Lau & Nath, 1996; Taschetto et al., 2020). This pattern is caused by anoma-
 343 lous tropical heating in the central Pacific during El Niño which excites atmospheric Rossby
 344 wave trains that propagate poleward and induce changes in atmospheric circulation and

345 surface heat fluxes. The Aleutian Low deepens during El Niño, resulting in anomalous
346 cold and dry northwesterly winds over the central North Pacific that cool SSTs and anoma-
347 lous warm and humid southeasterly winds over the eastern North Pacific that warm SSTs.
348 These changes in wind, air temperature, and humidity modulate the air-sea heat fluxes,
349 resulting in SST anomalies. These large-scale atmospheric patterns are evident in the
350 sea level pressure and 850-hPa wind regressed onto the Niño3.4 index (line contours and
351 vectors in Figure 2b, e, h).

352 The spatial pattern of the teleconnection in CESM2-LE for 1960-2000 is broadly
353 similar to the observed pattern but is displaced slightly to the west and is somewhat stronger
354 in magnitude. The westward displacement likely is due to the ENSO SST anomaly in
355 CESM2 extending further west than in observations (Chen et al., 2021). However, in most
356 of the North Pacific the observed teleconnection falls within two cross-ensemble stan-
357 dard deviations. At the center of action in the central North Pacific, the annually-averaged
358 teleconnection coefficient $\tilde{\beta}$ is much stronger in observations than in CESM2-LE for ei-
359 ther time period (see Figure S6 in the Supporting Information). However, the ensem-
360 ble mean Niño3.4 standard deviation in CESM2-LE is about 50% greater than in obser-
361 vations: 1.30 K and 1.26 K for 1960-2000 and 2060-2100, respectively, compared to the
362 observed value of 0.86 K for 1960-2000 in HadISST. Thus, the overall magnitude of forc-
363 ing of the teleconnection on SST anomalies is comparable between the model and ob-
364 servations.

365 In CESM2-LE, the ENSO teleconnection pattern shifts to the northeast in the fu-
366 ture climate. The teleconnection, both in its effect on atmospheric circulation and SSTs,
367 weakens slightly. That shift likely is caused by the eastward shift of the location of max-
368 imum precipitation during ENSO due to the expansion of the western Pacific warm pool
369 (see Power et al. (2013) and Yan et al. (2020)). Changes to the atmospheric waveguide
370 may also contribute to the teleconnection shift.

371 **3.3 Noise Forcing and Its Future Changes**

372 The variance of the noise forcing ξ has a broad maximum at 40°N in both the ob-
373 servations and CESM2-LE, stretching from Japan to about 150°W (Figure 2c, f, i). This
374 coincides with the subarctic SST front and the North Pacific storm track, thus high at-
375 mospheric and oceanic variability in this region is expected. The noise in observations

376 has considerably greater variance than in CESM2-LE even though the SST variance is
 377 similar. Because SST variance increases with increasing ocean memory (in an AR-1 pro-
 378 cess; see von Storch and Zwiers, 1999), the greater noise variance in observations is com-
 379 pensated by the somewhat shorter ocean memory to yield comparable overall SST vari-
 380 ance to CESM2-LE.

381 The future change of the noise forcing variance is spatially heterogeneous in CESM2-
 382 LE. Although increasing in most areas, particularly in the eastern North Pacific between
 383 Hawai'i and North America, there are areas in the central and southeastern parts of the
 384 basin where noise variance decreases. The strong increase in variance north of Japan is
 385 potentially due to a poleward shift of the Kuroshio (Yang et al., 2016).

386 3.4 Drivers of future SST Variance Change

387 As described in Section 2.5 we used the fitted values of $\tilde{\lambda}$, $\tilde{\beta}$, and ξ to create sev-
 388 eral sets of reconstituted SST data forced either by ENSO or by the noise residual ξ . The
 389 variance of the ENSO-forced SSTs is appreciably smaller than the noise-forced SSTs (Fig-
 390 ure 4b-c). However, the *change* in variance of the ENSO-forced SSTs due to the shift
 391 of the ENSO teleconnection is comparable in magnitude to the change in variance of the
 392 noise-forced SSTs (Figure 4e-f). The sum of the individual variance changes sums to close
 393 to the true variance change, supporting the validity of integrating the forcings separately
 394 (compare Figure 4a and g).

395 The pattern of variance change due to each of the three drivers closely resembles
 396 the changes to the corresponding parameters in Figure 2j-i. Increases in the ocean mem-
 397 ory lead to increased SST variance and vice versa, as expected for an AR-1 process (see
 398 von Storch and Zwiers, 1999). Likewise, increases in the magnitude of the ENSO tele-
 399 connection and noise forcing lead to increases in SST variance, and vice versa. The change
 400 in the strength of the ENSO teleconnection is almost entirely a function of the change
 401 in $\tilde{\beta}$ as the change in the Niño3.4 variance is small between the two time periods in CESM2-
 402 LE.

403 Figure 4h shows the contribution of each driver to the overall variance change by
 404 assigning the change due to each driver to a color channel (red= $\Delta^\xi \sigma^2(T')$, green= $\Delta^N \sigma^2(T')$,
 405 blue= $\Delta^\lambda \sigma^2(T')$). At each grid point, a driver was only considered to contribute to the
 406 change in variance if its associated variance change was of the same sign as the total SST

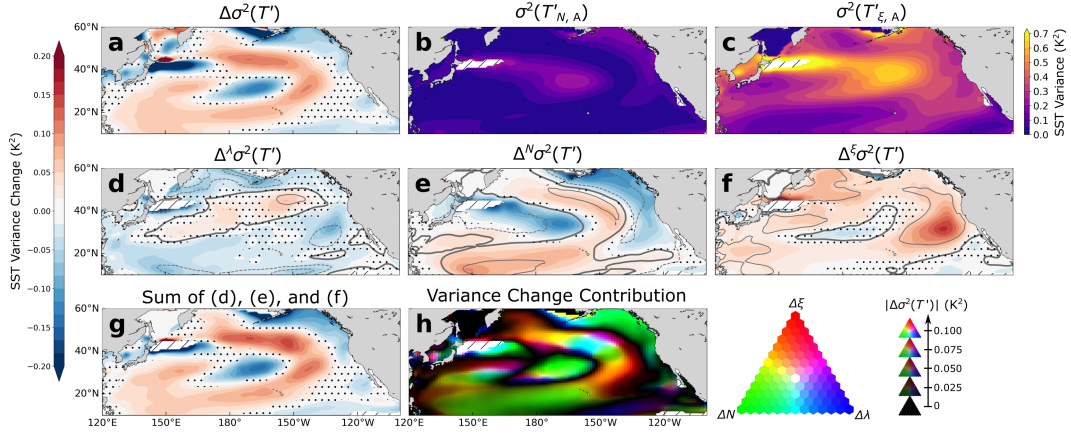


Figure 4. (a) The total SST variance change as in Figure 1c. (b) and (c) The SST variance associated with ENSO-only and noise-only forcing, respectively, for 1960-2000. (d)-(f) The SST variance changes associated with the change in ocean memory, the ENSO teleconnection, and stochastic noise. The grey contours represent the same changes as in Figure 2j-l: the change of the ocean memory $\tilde{\lambda}^{-1}$, ENSO teleconnection $\tilde{\beta}\sigma(\text{Niño3.4})$, and the noise variance $\sigma(\xi)$, respectively. The zero contour line is thicker, with contour intervals of 0.67 months, 0.04 K/month, and 0.02 K/month, respectively. (g) The total SST variance change computed by summing (d), (e), and (f). (h) The contribution of the change of each driver to the SST variance change. Hue indicates the relative contribution of each driver and brightness corresponds to the magnitude of the total SST variance change (see Figure S7 in the Supporting Information). Locations where the SST data does not meet the criterion described in Section 2.4 are shown as white hatched areas. Stippling indicates where the changes are not significant at the 5% level.

407 variance change (i.e., if at some grid point $\Delta\sigma^2(T') > 0$ and $\Delta^\lambda\sigma^2(T') < 0$, the change
 408 in $\tilde{\lambda}$ was considered to not contribute to the overall change in variance). Then the vari-
 409 ance of the drivers that do contribute to the SST variance change is represented by a mix
 410 of colors, with the hue signifying the relative contribution of each driver, and the bright-
 411 ness being proportional to the magnitude of the total SST variance change. The con-
 412 struction of this visualization is detailed in Figure S7 in the Supporting Information.

413 As evidenced by the large areas of green in Figure 4h, the shift of the ENSO tele-
 414 connection dominates the SST variance change pattern. The arcuate pattern in the central
 415 North Pacific and the decrease in variance in the Gulf of Alaska are almost entirely
 416 due to the shift in the teleconnection. The change in the stochastic noise forcing con-
 417 tributes to a lesser extent, with its greatest influence being northeast of Hawai'i. In most

418 of the North Pacific, decreased SST variance due to declining ocean memory is compen-
 419 sated for by increased variance due to increasing stochastic noise forcing. That mem-
 420 ory is generally declining and noise increasing implies that the “damped-persistence” pre-
 421 dictability of SST anomalies will decline in the future in most areas.

422 We also assessed the contribution of the change of each driver by using the pat-
 423 tern correlation, defined as the Pearson correlation coefficient between two arrays weighted
 424 by the cosine of the latitude. Areas of the arrays where the R_{TQ} criterion described in
 425 Section 2.4 are not met were removed. In the North Pacific (10°N-60°N, 120°E-100°W)
 426 the pattern correlations between the total variance change (as in Figure 4g) and the vari-
 427 ance changes due to individual drivers are 0.15 for $\Delta^\lambda \sigma^2(T')$, 0.76 for $\Delta^N \sigma^2(T')$, and
 428 0.47 for $\Delta^\xi \sigma^2(T')$. Those correlations support the above conclusion that the shift in the
 429 ENSO teleconnection is most important to the overall change in SST variance, followed
 430 by the change in the stochastic noise, with the change in ocean memory playing only a
 431 minor role.

432 4 Conclusions

433 In this work, we have demonstrated a conceptual model of SST variability that can
 434 explain the drivers behind future change of projected SST variance. By using this frame-
 435 work, we were able to quantify the SST variance change between 1960-2000 and 2060-
 436 2100 to three drivers:

- 437 • *Ocean Memory* – The ocean memory declines over most of the North Pacific with
 438 an elongated region in the center of the basin exhibiting longer memory in the fu-
 439 ture. We attribute this change primarily to changes in air-sea feedbacks and ocean
 440 damping, the latter presumably due to changes in horizontal diffusion and entrain-
 441 ment. The latent heat and shortwave feedbacks, the latter likely due to the low
 442 cloud-SST feedback, are the most important air-sea feedbacks. The shallowing mixed
 443 layer depth appears to play a secondary role. The change in ocean memory plays
 444 a minor role in the overall change in SST variance as its impact is largely com-
 445 pensated for by increases in stochastic noise forcing.
- 446 • *ENSO Teleconnections* – The “atmospheric bridge,” which connects North Pacific
 447 SSTs to ENSO events via atmospheric Rossby waves, shifts to the northeast in
 448 the future climate. Although the extratropical SST variance associated with re-

449 mote ENSO forcing is much smaller than the variance driven by stochastic noise,
450 the shift of the ENSO teleconnection pattern results in a large change in SST vari-
451 ance, dominating the overall change in SST variance.

- 452 • *Stochastic Noise Forcing* – The noise forcing, computed as a residual from a fit
453 to an extended local linear stochastic-deterministic model (equation 1), increases
454 in most of the North Pacific. Its impact on SST variance is somewhat attenuated
455 by the change in the ocean memory.

456 These findings have implications for predictability – the generally lower ocean mem-
457 ory and higher noise forcing suggests that predictability of a simple “damped persistence”
458 model will decline in skill in the future climate in most regions. ENSO is a major source
459 of SST predictability on seasonal timescales, hence the shift of its teleconnections results
460 in ENSO-associated changes in predictability in different regions. Our results highlight
461 the importance of studies into future ENSO changes and its regional impacts.

462 Although this study was focused narrowly on the North Pacific and the CESM2-
463 LE model, our framework should be equally applicable to other extratropical oceans and
464 other climate models. Different large ensemble climate models show considerable diver-
465 sity in their future ENSO dynamics (Maher et al., 2023), thus contribution of the var-
466 ious drivers of SST variability may differ greatly between models. This study also did
467 not determine the physical mechanisms responsible for the change in ocean memory and
468 stochastic noise forcing and how they relate to climate mean state changes. We aim to
469 answer these questions in future work.

470 **Data Availability Statement**

471 The CESM2-LE data are available via the Earth System Grid ([https://www.earthsystemgrid](https://www.earthsystemgrid.org)
472 [.org](https://www.earthsystemgrid.org)), the HadISST data are available from the Met Office ([https://www.metoffice](https://www.metoffice.gov.uk/hadobs/hadisst/)
473 [.gov.uk/hadobs/hadisst/](https://www.metoffice.gov.uk/hadobs/hadisst/)), the ERA5 and ORAS5 data are available via the Climate
474 Data Store (<https://cds.climate.copernicus.eu>), the OAFLUX data are available
475 from WHOI (<https://oaf Flux.whoi.edu/>), and the CERES data are available from NASA
476 (<https://ceres.larc.nasa.gov/>). The code and data required to reproduce the fig-
477 ures is available via Zenodo (<https://doi.org/10.5281/zenodo.10419764>).

Conflict of Interest Statement

The authors have no conflicts of interest to declare.

Acknowledgments

This study was supported by NOAA’s Climate Program Office’s Modeling, Analysis, Predictions, and Projections (MAPP) program under grant NA20OAR4310445 and NSF grant AGS-2141728. JLG acknowledges the support of the Uehiro Center for the Advancement of Oceanography. MFS participates in the MAPP Marine Ecosystem Task Force. The authors acknowledge helpful discussions with Fei-Fei Jin, Niklas Schneider, and Brian Powell. The CESM2-LE simulations were conducted on the Aleph supercomputer through a partnership between the Institute for Basic Sciences (IBS) Center for Climate Physics (ICCP) in South Korea and the CESM group at the National Center for Atmospheric Research (NCAR) in the U.S., representing a broad collaborative effort between scientists from both centers. Special thanks goes to Axel Timmermann, Keith Rodgers, Sun-Seon Lee, Nan Rosenbloom, and Jim Edwards from those institutions. This is IPRC publication X and SOEST contribution Y.

References

- Alexander, M. A., Bladé, I., Newman, M., Lanzante, J. R., Lau, N.-C., & Scott, J. D. (2002). The Atmospheric Bridge: The Influence of ENSO Teleconnections on Air–Sea Interaction over the Global Oceans. *Journal of Climate*, *15*(16), 2205–2231. [https://doi.org/10.1175/1520-0442\(2002\)015<2205:TABTIO>2.0.CO;2](https://doi.org/10.1175/1520-0442(2002)015<2205:TABTIO>2.0.CO;2)
- Alexander, M. A., & Deser, C. (1995). A Mechanism for the Recurrence of Wintertime Midlatitude SST Anomalies. *Journal of Physical Oceanography*, *25*(1), 122–137. [https://doi.org/10.1175/1520-0485\(1995\)025%3C0122:AMFTR0%3E2.0.CO;2](https://doi.org/10.1175/1520-0485(1995)025%3C0122:AMFTR0%3E2.0.CO;2)
- Amaya, D. J., Jacox, M. G., Fewings, M. R., Saba, V. S., Stuecker, M. F., Rykaczewski, R. R., Ross, A. C., Stock, C. A., Capotondi, A., Petrik, C. M., Bograd, S. J., Alexander, M. A., Cheng, W., Hermann, A. J., Kearney, K. A., & Powell, B. S. (2023). Marine heatwaves need clear definitions so coastal communities can adapt. *Nature*, *616*(7955), 29–32. <https://doi.org/10.1038/d41586-023-00924>

- 508 Bui, H. X., & Maloney, E. D. (2018). Changes in Madden-Julian Oscillation Precipitation
509 and Wind Variance Under Global Warming. *Geophysical Research Letters*,
510 *45*(14), 7148–7155. <https://doi.org/10.1029/2018GL078504>
- 511 Bui, H. X., & Maloney, E. D. (2020). Changes to the Madden-Julian Oscillation in Cou-
512 pled and Uncoupled Aquaplanet Simulations With 4xCO₂. *Journal of Advances
513 in Modeling Earth Systems*, *12*(8). <https://doi.org/10.1029/2020MS002179>
- 514 Cai, W., Santoso, A., Wang, G., Wu, L., Collins, M., Lengaigne, M., Power, S., & Tim-
515 mermann, A. (2020). ENSO Response to Greenhouse Forcing. In M. J. McPhaden,
516 A. Santoso, & W. Cai (Eds.), *Geophysical Monograph Series* (1st ed., pp. 289–
517 307). Wiley. <https://doi.org/10.1002/9781119548164.ch13>
- 518 Cai, W., Wang, G., Dewitte, B., Wu, L., Santoso, A., Takahashi, K., Yang, Y., Carréric,
519 A., & McPhaden, M. J. (2018). Increased variability of eastern Pacific El Niño
520 under greenhouse warming. *Nature*, *564*(7735), 201–206. [https://doi.org/
521 10.1038/s41586-018-0776-9](https://doi.org/10.1038/s41586-018-0776-9)
- 522 Capotondi, A., Alexander, M. A., Bond, N. A., Curchitser, E. N., & Scott, J. D. (2012).
523 Enhanced upper ocean stratification with climate change in the CMIP3 mod-
524 els. *Journal of Geophysical Research: Oceans*, *117*(C4). [https://doi.org/
525 10.1029/2011JC007409](https://doi.org/10.1029/2011JC007409)
- 526 Chen, H.-C., Fei-Fei-Jin, Zhao, S., Wittenberg, A. T., & Xie, S. (2021). ENSO Dynam-
527 ics in the E3SM-1-0, CESM2, and GFDL-CM4 Climate Models. *Journal of Cli-
528 mate*, *34*(23), 9365–9384. <https://doi.org/10.1175/JCLI-D-21-0355.1>
- 529 Clement, A. C., Burgman, R., & Norris, J. R. (2009). Observational and Model Evidence
530 for Positive Low-Level Cloud Feedback. *Science*, *325*(5939), 460–464. [https://
531 //doi.org/10.1126/science.1171255](https://doi.org/10.1126/science.1171255)
- 532 Danabasoglu, G., Lamarque, J.-F., Bacmeister, J., Bailey, D. A., DuVivier, A. K., Ed-
533 wards, J., Emmons, L. K., Fasullo, J., Garcia, R., Gettelman, A., Hannay, C.,
534 Holland, M. M., Large, W. G., Lauritzen, P. H., Lawrence, D. M., Lenaerts, J. T. M.,
535 Lindsay, K., Lipscomb, W. H., Mills, M. J., ... Strand, W. G. (2020). The Com-
536 munity Earth System Model Version 2 (CESM2). *Journal of Advances in Mod-
537 eling Earth Systems*, *12*(2). <https://doi.org/10.1029/2019MS001916>
- 538 De Elvira, A. R., & Lemke, P. (1982). A Langevin equation for stochastic climate mod-
539 els with periodic feedback and forcing variance. *Tellus*, *34*(4), 313–320. [https://
540 //doi.org/10.1111/j.2153-3490.1982.tb01821.x](https://doi.org/10.1111/j.2153-3490.1982.tb01821.x)

- 541 Delworth, T. L., & Greatbatch, R. J. (2000). Multidecadal Thermohaline Circulation Vari-
 542 ability Driven by Atmospheric Surface Flux Forcing. *Journal of Climate*, *13*(9),
 543 1481–1495. [https://doi.org/10.1175/1520-0442\(2000\)013<1481:
 544 MTCVDB>2.0.CO;2](https://doi.org/10.1175/1520-0442(2000)013<1481:MTCVDB>2.0.CO;2)
- 545 Deser, C., Lehner, F., Rodgers, K. B., Ault, T., Delworth, T. L., DiNezio, P. N., Fiore,
 546 A., Frankignoul, C., Fyfe, J. C., Horton, D. E., Kay, J. E., Knutti, R., Loven-
 547 duski, N. S., Marotzke, J., McKinnon, K. A., Minobe, S., Randerson, J., Screen,
 548 J. A., Simpson, I. R., & Ting, M. (2020). Insights from Earth system model initial-
 549 condition large ensembles and future prospects. *Nature Climate Change*, *10*(4),
 550 277–286. <https://doi.org/10.1038/s41558-020-0731-2>
- 551 Deser, C., Alexander, M. A., & Timlin, M. S. (2003). Understanding the Persistence of
 552 Sea Surface Temperature Anomalies in Midlatitudes. *Journal of Climate*, *16*(1),
 553 57–72. [https://doi.org/10.1175/1520-0442\(2003\)016<0057:UTPOSS>2.0
 554 .CO;2](https://doi.org/10.1175/1520-0442(2003)016<0057:UTPOSS>2.0)
- 555 Deser, C., Alexander, M. A., Xie, S.-P., & Phillips, A. S. (2010). Sea Surface Temper-
 556 ature Variability: Patterns and Mechanisms. *Annual Review of Marine Science*,
 557 *2*(1), 115–143. [https://doi.org/10.1146/annurev-
 558 -151453](https://doi.org/10.1146/annurev-marine-120408)
- 559 Frankignoul, C., & Kestenare, E. (2002). The surface heat flux feedback. Part I: Esti-
 560 mates from observations in the Atlantic and the North Pacific. *Climate Dynam-*
 561 *ics*, *19*(8), 633–647. <https://doi.org/10.1007/s00382-002-0252-x>
- 562 Frankignoul, C., Kestenare, E., & Mignot, J. (2002). The surface heat flux feedback. Part
 563 II: Direct and indirect estimates in the ECHAM4/OPA8 coupled GCM. *Climate*
 564 *Dynamics*, *19*(8), 649–655. <https://doi.org/10.1007/s00382-002-0253-9>
- 565 Frankignoul, C. (1985). Sea surface temperature anomalies, planetary waves, and air-
 566 sea feedback in the middle latitudes. *Reviews of Geophysics*, *23*(4), 357. [https:
 567 //doi.org/10.1029/RG023i004p00357](https://doi.org/10.1029/RG023i004p00357)
- 568 Frankignoul, C., & Hasselmann, K. (1977). Stochastic climate models. Part II: Appli-
 569 cation to sea-surface temperature anomalies and thermocline variability. *Tellus*,
 570 *29*(4), 289–305. <https://doi.org/10.1111/j.2153-3490.1977.tb00740.x>
- 571 Frankignoul, C., & Reynolds, R. W. (1983). Testing a Dynamical Model for Mid-Latitude
 572 Sea Surface Temperature Anomalies. *Journal of Physical Oceanography*, *13*(7),

- 573 1131–1145. [https://doi.org/10.1175/1520-0485\(1983\)013%3C1131:](https://doi.org/10.1175/1520-0485(1983)013%3C1131:TADMFM%3E2.0.CO;2)
574 [TADMFM%3E2.0.CO;2](https://doi.org/10.1175/1520-0485(1983)013%3C1131:TADMFM%3E2.0.CO;2)
- 575 Geng, T., Cai, W., Wu, L., Santoso, A., Wang, G., Jing, Z., Gan, B., Yang, Y., Li, S.,
576 Wang, S., Chen, Z., & McPhaden, M. J. (2022). Emergence of changing Central-
577 Pacific and Eastern-Pacific El Niño-Southern Oscillation in a warming climate.
578 *Nature Communications*, *13*(1), 6616. [https://doi.org/10.1038/s41467-](https://doi.org/10.1038/s41467-022-33930-5)
579 [-022-33930-5](https://doi.org/10.1038/s41467-022-33930-5)
- 580 Hall, A., & Manabe, S. (1997). Can local linear stochastic theory explain sea surface tem-
581 perature and salinity variability? *Climate Dynamics*, *13*(3), 167–180. [https:](https://doi.org/10.1007/s003820050158)
582 [//doi.org/10.1007/s003820050158](https://doi.org/10.1007/s003820050158)
- 583 Haney, R. L. (1971). Surface Thermal Boundary Condition for Ocean Circulation Mod-
584 els. *Journal of Physical Oceanography*, *1*(4), 241–248. [https://doi.org/10](https://doi.org/10.1175/1520-0485(1971)001<0241:STBCF0>2.0.CO;2)
585 [.1175/1520-0485\(1971\)001<0241:STBCF0>2.0.CO;2](https://doi.org/10.1175/1520-0485(1971)001<0241:STBCF0>2.0.CO;2)
- 586 Hasselmann, K. (1976). Stochastic climate models. Part I: Theory. *Tellus*, *28*(6), 473–
587 485. <https://doi.org/10.1111/j.2153-3490.1976.tb00696.x>
- 588 Hawkins, E., & Sutton, R. (2009). The Potential to Narrow Uncertainty in Regional Cli-
589 mate Predictions. *Bulletin of the American Meteorological Society*, *90*(8), 1095–
590 1108. <https://doi.org/10.1175/2009BAMS2607.1>
- 591 Hersbach, H., Bell, B., Berrisford, P., Hirahara, S., Horányi, A., Muñoz-Sabater, J., Nico-
592 las, J., Peubey, C., Radu, R., Schepers, D., Simmons, A., Soci, C., Abdalla, S.,
593 Abellan, X., Balsamo, G., Bechtold, P., Biavati, G., Bidlot, J., Bonavita, M., ...
594 Thépaut, J.-N. (2020). The ERA5 global reanalysis. *Quarterly Journal of the*
595 *Royal Meteorological Society*, *146*(730), 1999–2049. [https://doi.org/10](https://doi.org/10.1002/qj.3803)
596 [.1002/qj.3803](https://doi.org/10.1002/qj.3803)
- 597 Jacox, M. G., Alexander, M. A., Bograd, S. J., & Scott, J. D. (2020). Thermal displace-
598 ment by marine heatwaves. *Nature*, *584*(7819), 82–86. [https://doi.org/10](https://doi.org/10.1038/s41586-020-2534-z)
599 [.1038/s41586-020-2534-z](https://doi.org/10.1038/s41586-020-2534-z)
- 600 Jenney, A. M., Randall, D. A., & Barnes, E. A. (2021). Drivers of uncertainty in future
601 projections of Madden–Julian Oscillation teleconnections. *Weather and Climate*
602 *Dynamics*, *2*(3), 653–673. <https://doi.org/10.5194/wcd-2-653-2021>
- 603 Kato, S., Rose, F. G., Rutan, D. A., Thorsen, T. J., Loeb, N. G., Doelling, D. R., Huang,
604 X., Smith, W. L., Su, W., & Ham, S.-H. (2018). Surface Irradiances of Edition
605 4.0 Clouds and the Earth’s Radiant Energy System (CERES) Energy Balanced

- 606 and Filled (EBAF) Data Product. *Journal of Climate*, *31*(11), 4501–4527. <https://doi.org/10.1175/JCLI-D-17-0523.1>
- 607
- 608 Large, W. G., Danabasoglu, G., Doney, S. C., & McWilliams, J. C. (1997). Sensitivity
609 to Surface Forcing and Boundary Layer Mixing in a Global Ocean Model: Annual-
610 Mean Climatology. *Journal of Physical Oceanography*, *27*(11), 2418–2447. [https://doi.org/10.1175/1520-0485\(1997\)027<2418:STSFAB>2.0.CO;2](https://doi.org/10.1175/1520-0485(1997)027<2418:STSFAB>2.0.CO;2)
- 611
- 612 Larson, S. M., Vimont, D. J., Clement, A. C., & Kirtman, B. P. (2018). How Momen-
613 tum Coupling Affects SST Variance and Large-Scale Pacific Climate Variabil-
614 ity in CESM. *Journal of Climate*, *31*(7), 2927–2944. <https://doi.org/10.1175/JCLI-D-17-0645.1>
- 615
- 616 Lau, N.-C., & Nath, M. J. (1996). The Role of the “Atmospheric Bridge” in Linking Trop-
617 ical Pacific ENSO Events to Extratropical SST Anomalies. *Journal of Climate*,
618 *9*(9), 2037–2057. [https://doi.org/10.1175/1520-0442\(1996\)009<2036:TROTBI>2.0.CO;2](https://doi.org/10.1175/1520-0442(1996)009<2036:TROTBI>2.0.CO;2)
- 619
- 620 Li, W., Pan, R., Jiang, Z., Chen, Y., Li, L., Luo, J.-J., Zhai, P., Shen, Y., & Yu, J. (2021).
621 Future changes in the frequency of extreme droughts over China based on two
622 large ensemble simulations. *Journal of Climate*, *34*(14), 6023–6035. <https://doi.org/10.1175/JCLI-D-20-0656.1>
- 623
- 624 Lorenz, E. N. (1963). Deterministic Nonperiodic Flow. *Journal of the Atmospheric Sci-*
625 *ences*, *20*(2), 130–141. [https://doi.org/10.1175/1520-0469\(1963\)020<0130:DNF>2.0.CO;2](https://doi.org/10.1175/1520-0469(1963)020<0130:DNF>2.0.CO;2)
- 626
- 627 Maher, N., Milinski, S., Suarez-Gutierrez, L., Botzet, M., Dobrynin, M., Kornblueh, L.,
628 Kröger, J., Takano, Y., Ghosh, R., Hedemann, C., Li, C., Li, H., Manzini, E.,
629 Notz, D., Putrasahan, D., Boysen, L., Claussen, M., Ilyina, T., Olonscheck, D.,
630 ... Marotzke, J. (2019). The Max Planck Institute Grand Ensemble: Enabling
631 the Exploration of Climate System Variability. *Journal of Advances in Model-*
632 *ing Earth Systems*, *11*(7), 2050–2069. <https://doi.org/10.1029/2019MS001639>
- 633
- 634 Maher, N., Wills, R. C. J., DiNezio, P., Klavans, J., Milinski, S., Sanchez, S. C., Steven-
635 son, S., Stuecker, M. F., & Wu, X. (2023). The future of the El Niño–Southern
636 Oscillation: Using large ensembles to illuminate time-varying responses and inter-
637 model differences. *Earth System Dynamics*, *14*(2), 413–431. <https://doi.org/10.5194/esd-14-413-2023>

- 638 Manabe, S., & Wetherald, R. T. (1967). Thermal Equilibrium of the Atmosphere with
639 a Given Distribution of Relative Humidity. *Journal of the Atmospheric Sciences*,
640 *24*(3), 241–259. [https://doi.org/10.1175/1520-0469\(1967\)024<0241:
641 TEOTAW>2.0.CO;2](https://doi.org/10.1175/1520-0469(1967)024<0241:TEOTAW>2.0.CO;2)
- 642 Newman, M., Alexander, M. A., Ault, T. R., Cobb, K. M., Deser, C., Di Lorenzo, E.,
643 Mantua, N. J., Miller, A. J., Minobe, S., Nakamura, H., Schneider, N., Vimont,
644 D. J., Phillips, A. S., Scott, J. D., & Smith, C. A. (2016). The Pacific Decadal
645 Oscillation, Revisited. *Journal of Climate*, *29*(12), 4399–4427. [https://doi
646 .org/10.1175/JCLI-D-15-0508.1](https://doi.org/10.1175/JCLI-D-15-0508.1)
- 647 Newman, M., Compo, G. P., & Alexander, M. A. (2003). ENSO-Forced Variability of
648 the Pacific Decadal Oscillation. *Journal of Climate*, *16*(23), 3853–3857. [https:
649 //doi.org/10.1175/1520-0442\(2003\)016<3853:EVOTPD>2.0.CO;2](https://doi.org/10.1175/1520-0442(2003)016<3853:EVOTPD>2.0.CO;2)
- 650 Nicholls, N. (1984). The Southern Oscillation and Indonesian Sea Surface Temperature.
651 *Monthly Weather Review*, *112*(3), 424–432. [https://doi.org/10.1175/
652 1520-0493\(1984\)112<0424:TSOAIS>2.0.CO;2](https://doi.org/10.1175/1520-0493(1984)112<0424:TSOAIS>2.0.CO;2)
- 653 Norris, J. R., & Leovy, C. B. (1994). Interannual Variability in Stratiform Cloudiness
654 and Sea Surface Temperature. *Journal of Climate*, *7*(12), 1915–1925. [https:
655 //doi.org/10.1175/1520-0442\(1994\)007<1915:IVISCA>2.0.CO;2](https://doi.org/10.1175/1520-0442(1994)007<1915:IVISCA>2.0.CO;2)
- 656 Nummelin, A., Busecke, J. J. M., Haine, T. W. N., & Abernathy, R. P. (2021). Diag-
657 nosing the Scale- and Space-Dependent Horizontal Eddy Diffusivity at the Global
658 Surface Ocean. *Journal of Physical Oceanography*, *51*(2), 279–297. [https://
659 doi.org/10.1175/JPO-D-19-0256.1](https://doi.org/10.1175/JPO-D-19-0256.1)
- 660 Oliver, E. C., Benthuisen, J. A., Darmaraki, S., Donat, M. G., Hobday, A. J., Holbrook,
661 N. J., Schlegel, R. W., & Sen Gupta, A. (2021). Marine Heatwaves. *Annual Re-
662 view of Marine Science*, *13*(1), 313–342. [https://doi.org/10.1146/annurev
663 -marine-032720-095144](https://doi.org/10.1146/annurev-marine-032720-095144)
- 664 Patrizio, C. R., & Thompson, D. W. J. (2021). Quantifying the Role of Ocean Dynam-
665 ics in Ocean Mixed Layer Temperature Variability. *Journal of Climate*, *34*(7),
666 2567–2589. <https://doi.org/10.1175/JCLI-D-20-0476.1>
- 667 Patrizio, C. R., & Thompson, D. W. J. (2022). Understanding the Role of Ocean Dy-
668 namics in Midlatitude Sea Surface Temperature Variability Using a Simple Stochas-
669 tic Climate Model. *Journal of Climate*, *35*(11), 3313–3333. [https://doi.org/
670 10.1175/JCLI-D-21-0184.1](https://doi.org/10.1175/JCLI-D-21-0184.1)

- 671 Power, S., Delage, F., Chung, C., Kociuba, G., & Keay, K. (2013). Robust twenty-first-
 672 century projections of El Niño and related precipitation variability. *Nature*, *502*(7472),
 673 541–545. <https://doi.org/10.1038/nature12580>
- 674 Qiu, B. (2002). The Kuroshio Extension System: Its Large-Scale Variability and Role
 675 in the Midlatitude Ocean-Atmosphere Interaction. *Journal of Oceanography*, *58*(1),
 676 57–75. <https://doi.org/10.1023/A:1015824717293>
- 677 Rayner, N. A. (2003). Global analyses of sea surface temperature, sea ice, and night ma-
 678 rine air temperature since the late nineteenth century. *Journal of Geophysical*
 679 *Research*, *108*(D14), 4407. <https://doi.org/10.1029/2002JD002670>
- 680 Reynolds, R. W. (1978). Sea surface temperature anomalies in the North Pacific Ocean.
 681 *Tellus*, *30*(2), 97–103. [https://doi.org/10.1111/j.2153-3490.1978](https://doi.org/10.1111/j.2153-3490.1978.tb00822.x)
 682 [.tb00822.x](https://doi.org/10.1111/j.2153-3490.1978.tb00822.x)
- 683 Rodgers, K. B., Lee, S.-S., Rosenbloom, N., Timmermann, A., Danabasoglu, G., Deser,
 684 C., Edwards, J., Kim, J.-E., Simpson, I. R., Stein, K., Stuecker, M. F., Yamaguchi,
 685 R., Bódai, T., Chung, E.-S., Huang, L., Kim, W. M., Lamarque, J.-F., Lombar-
 686 dozzi, D. L., Wieder, W. R., & Yeager, S. G. (2021). Ubiquity of human-induced
 687 changes in climate variability. *Earth System Dynamics*, *12*(4), 1393–1411. <https://doi.org/10.5194/esd-12-1393-2021>
- 688
 689 Rossow, W. B., & Schiffer, R. A. (1999). Advances in Understanding Clouds from IS-
 690 CCP. *Bulletin of the American Meteorological Society*, *80*(11), 2261–2288. [https://doi.org/10.1175/1520-0477\(1999\)080<2261:AIUCFI>2.0.CO;2](https://doi.org/10.1175/1520-0477(1999)080<2261:AIUCFI>2.0.CO;2)
- 691
 692 Rushley, S. S., Kim, D., & Adames, Á. F. (2019). Changes in the MJO under Greenhouse
 693 Gas-Induced Warming in CMIP5 Models. *Journal of Climate*, *32*(3), 803–821.
 694 <https://doi.org/10.1175/JCLI-D-18-0437.1>
- 695
 696 Schneider, N., & Cornuelle, B. D. (2005). The Forcing of the Pacific Decadal Oscillation.
 697 *Journal of Climate*, *18*(21), 4355–4373. [https://doi.org/10.1175/JCLI3527](https://doi.org/10.1175/JCLI3527.1)
 698 [.1](https://doi.org/10.1175/JCLI3527.1)
- 699
 700 Schneider, N., & Miller, A. J. (2001). Predicting Western North Pacific Ocean Climate.
 701 *Journal of Climate*, *14*(20), 3997–4002. [https://doi.org/10.1175/1520-0442\(2001\)014<3997:PWNPOC>2.0.CO;2](https://doi.org/10.1175/1520-0442(2001)014<3997:PWNPOC>2.0.CO;2)
- 702
 703 Shi, H., Jin, F.-F., Wills, R. C. J., Jacox, M. G., Amaya, D. J., Black, B. A., Rykaczewski,
 704 R. R., Bograd, S. J., García-Reyes, M., & Sydeman, W. J. (2022). Global de-

- 703 cline in ocean memory over the 21st century. *Science Advances*, 8(18), eabm3468.
704 <https://doi.org/10.1126/sciadv.abm3468>
- 705 Smith, K. E., Burrows, M. T., Hobday, A. J., King, N. G., Moore, P. J., Sen Gupta, A.,
706 Thomsen, M. S., Wernberg, T., & Smale, D. A. (2023). Biological Impacts of Ma-
707 rine Heatwaves. *Annual Review of Marine Science*, 15(1), 119–145. [https://](https://doi.org/10.1146/annurev-marine-032122-121437)
708 doi.org/10.1146/annurev-marine-032122-121437
- 709 Smith, K. E., Burrows, M. T., Hobday, A. J., Sen Gupta, A., Moore, P. J., Thomsen,
710 M., Wernberg, T., & Smale, D. A. (2021). Socioeconomic impacts of marine heat-
711 waves: Global issues and opportunities. *Science*, 374(6566), eabj3593. [https:](https://doi.org/10.1126/science.abj3593)
712 [//doi.org/10.1126/science.abj3593](https://doi.org/10.1126/science.abj3593)
- 713 Stouffer, R. J., & Wetherald, R. T. (2007). Changes of Variability in Response to Increas-
714 ing Greenhouse Gases. Part I: Temperature. *Journal of Climate*, 20(21), 5455–
715 5467. <https://doi.org/10.1175/2007JCLI1384.1>
- 716 Stuecker, M. F. (2023). The climate variability trio: Stochastic fluctuations, El Niño, and
717 the seasonal cycle. *Geoscience Letters*, 10(1), 51. [https://doi.org/10.1186/](https://doi.org/10.1186/s40562-023-00305-7)
718 [s40562-023-00305-7](https://doi.org/10.1186/s40562-023-00305-7)
- 719 Stuecker, M. F., Timmermann, A., Jin, F.-F., Chikamoto, Y., Zhang, W., Wittenberg,
720 A. T., Widiastih, E., & Zhao, S. (2017). Revisiting ENSO/Indian Ocean Dipole
721 phase relationships. *Geophysical Research Letters*, 44(5), 2481–2492. [https://](https://doi.org/10.1002/2016GL072308)
722 doi.org/10.1002/2016GL072308
- 723 Taschetto, A. S., Ummenhofer, C. C., Stuecker, M. F., Dommenges, D., Ashok, K., Ro-
724 drigues, R. R., & Sang-Wook, Y. (2020). ENSO Atmospheric Teleconnections.
725 In *El Niño southern oscillation in a changing climate* (First Edition, pp. 311–
726 335). Wiley-American Geophysical Union.
- 727 Timmermann, A., Oberhuber, J., Bacher, A., Esch, M., Latif, M., & Roeckner, E. (1999).
728 Increased El Niño frequency in a climate model forced by future greenhouse warm-
729 ing. *Nature*, 398. <https://doi.org/10.1038/19505>
- 730 van der Wiel, K., & Bintanja, R. (2021). Contribution of climatic changes in mean and
731 variability to monthly temperature and precipitation extremes. *Communications*
732 *Earth & Environment*, 2(1), 1. [https://doi.org/10.1038/s43247-020](https://doi.org/10.1038/s43247-020-00077-4)
733 [-00077-4](https://doi.org/10.1038/s43247-020-00077-4)
- 734 von Storch, H., & Zwiers, F. W. (1999). *Statistical Analysis in Climate Research*. Cam-
735 bridge University Press.

- 736 Welch, B. L. (1947). The Generalization of ‘Student’s’ Problem when Several Different
737 Population Variances are Involved. *Biometrika*, *34*(1/2), 28. [https://doi.org/](https://doi.org/10.2307/2332510)
738 [10.2307/2332510](https://doi.org/10.2307/2332510)
- 739 Wengel, C., Lee, S.-S., Stuecker, M. F., Timmermann, A., Chu, J.-E., & Schloesser, F.
740 (2021). Future high-resolution El Niño/Southern Oscillation dynamics. *Nature*
741 *Climate Change*, *11*(9), 758–765. [https://doi.org/10.1038/s41558-021](https://doi.org/10.1038/s41558-021-01132-4)
742 [-01132-4](https://doi.org/10.1038/s41558-021-01132-4)
- 743 Xie, S.-P. (2023). *Coupled Atmosphere-Ocean Dynamics: From El Niño to Climate Change*.
744 Elsevier.
- 745 Yan, Z., Wu, B., Li, T., Collins, M., Clark, R., Zhou, T., Murphy, J., & Tan, G. (2020).
746 Eastward shift and extension of ENSO-induced tropical precipitation anom-
747 lies under global warming. *Science Advances*, *6*(2), eaax4177. [https://doi](https://doi.org/10.1126/sciadv.aax4177)
748 [.org/10.1126/sciadv.aax4177](https://doi.org/10.1126/sciadv.aax4177)
- 749 Yang, H., Lohmann, G., Wei, W., Dima, M., Ionita, M., & Liu, J. (2016). Intensification
750 and poleward shift of subtropical western boundary currents in a warming cli-
751 mate. *Journal of Geophysical Research: Oceans*, *121*(7), 4928–4945. [https://](https://doi.org/10.1002/2015JC011513)
752 doi.org/10.1002/2015JC011513
- 753 Ying, J., Collins, M., Cai, W., Timmermann, A., Huang, P., Chen, D., & Stein, K. (2022).
754 Emergence of climate change in the tropical Pacific. *Nature Climate Change*, *12*(4),
755 356–364. <https://doi.org/10.1038/s41558-022-01301-z>
- 756 Yu, L., & Weller, R. A. (2007). Objectively Analyzed Air–Sea Heat Fluxes for the Global
757 Ice-Free Oceans (1981–2005). *Bulletin of the American Meteorological Society*,
758 *88*(4), 527–540. <https://doi.org/10.1175/BAMS-88-4-527>
- 759 Zhang, R., Sutton, R., Danabasoglu, G., Kwon, Y.-O., Marsh, R., Yeager, S. G., Am-
760 rhein, D. E., & Little, C. M. (2019). A Review of the Role of the Atlantic Merid-
761 ional Overturning Circulation in Atlantic Multidecadal Variability and Associ-
762 ated Climate Impacts. *Reviews of Geophysics*, *57*(2), 316–375. [https://doi](https://doi.org/10.1029/2019RG000644)
763 [.org/10.1029/2019RG000644](https://doi.org/10.1029/2019RG000644)
- 764 Zhao, S., Jin, F.-F., & Stuecker, M. F. (2019). Improved Predictability of the Indian Ocean
765 Dipole Using Seasonally Modulated ENSO Forcing Forecasts. *Geophysical Re-*
766 *search Letters*, *46*(16), 9980–9990. <https://doi.org/10.1029/2019GL084196>
- 767 Zuo, H., Balmaseda, M. A., Tietsche, S., Mogensen, K., & Mayer, M. (2019). The ECMWF
768 operational ensemble reanalysis–analysis system for ocean and sea ice: A descrip-

769 tion of the system and assessment. *Ocean Science*, 15(3), 779–808. [https://](https://doi.org/10.5194/os-15-779-2019)
770 doi.org/10.5194/os-15-779-2019